Published OnlineFirst on November 9, 2010 as 10.1158/0008-5472.CAN-10-2746

Cancer Research

MicroRNA miR-302 Inhibits the Tumorigenecity of Human Pluripotent Stem Cells by Coordinate Suppression of the CDK2 and CDK4/6 Cell Cycle Pathways

Shi-Lung Lin[1], Donald C. Chang[1], Shao-Yao Ying[2], Davey Leu[1], and David T.S. Wu[1]

Abstract

miR-302 is the major microRNA found in human embryonic stem cells and induced pluripotent stem cells, but its function has been unclear. In mice, there is evidence that miR-302 may silence p21Cip1 (CDKN1A) to promote cell proliferation, whereas studies in human reprogrammed pluripotent stem cells suggested that elevated miR-302 expression inhibited cell cycle transit. Here, we clarify this difference, reporting that in human cells, miR-302 simultaneously suppressed both the cyclin E-CDK2 and cyclin D-CDK4/6 pathways to block >70% of the G_1-S cell cycle transition. Concurrent silencing of BMI-1, a cancer stem cell marker targeted by miR-302, further promoted tumor suppressor functions of p16Ink4a and p14/p19Arf directed against CDK4/6–mediated cell proliferation. Among all G_1 phase checkpoint regulators, human p21Cip1 was found not to be a valid target of miR-302. Overall, our findings indicate that miR-302 inhibits human pluripotent stem cell tumorigenicity by enhancing multiple G_1 phase arrest pathways rather than by silencing p21Cip1. *Cancer Res; 70(22); 9473–82. ©2010 AACR.*

Introduction

Previous studies have shown that ectopic expression of miR-302 is able to reprogram human cancer cells to human embryonic stem cell (hESC)–like pluripotent cells with a distinct slow cell cycle rate and dormant cell-like morphology (1, 2). Relative quiescence is a defined characteristic of these miR-302–reprogrammed pluripotent stem cells (mirPSC), whereas other three-/four-factor (*Oct4-Sox2-Klf4-c-Myc* or *Oct4-Sox2-Nanog-Lin28*)–induced iPSCs have dramatic proliferative ability and inexorable tumorigenic tendency (3–5). Although the mechanism underlying such a difference is still unclear, we and others have identified two involved G_1-phase checkpoint regulators, cyclin-dependent kinase 2 (CDK2) and cyclin D (1, 6). Progression in the eukaryotic cell cycle is driven by the formation of functional complexes between cyclin-dependent kinases (CDK) and cyclins. Negative regulators, such as CDK inhibitors, suppress the activities of cyclin-CDK complexes to hinder cell proliferation. Major CDK inhibitors include p15Ink4b, p16Ink4a, p18Ink4c, p21Cip1/Waf1, and p27Kip1. In mammalian cells, different cyclin-CDK complexes are involved in regulating different cell cycle transitions, such as cyclin D-CDK4/6 for G_1 progression, cyclin E-CDK2 for G_1-S transition, cyclin A-CDK2 for S-phase progression, and cyclin A/B-CDC2 (cyclin A/B-CDK1) for M-phase entry. Thus, it is conceivable that the antiproliferative function of miR-302 may result from the concurrent suppression of CDK2 and cyclin D during the G_1-S cell cycle transition.

However, studies of the miR-291/294/295 family, an analogue to human miR-302 in mouse, revealed a different result from the miR-302 function in human mirPSCs. In mouse embryonic stem cells (mESC), ectopic expression of miR-291/294/295 promoted fast cell proliferation and G_1-S cell cycle transition through direct silencing of p21Cip1 (also named CDKN1A) and the serine/threonine-protein kinase Lats2 (7). Transgenic mice lacking p21Cip1/Waf1 were shown to display normal development with a defect in the G_1-phase checkpoint control (8). Yet, the role of Lats2 remains to be determined because of its function in the recruitment of γ-tubulin and spindle formation at the onset of mitosis. Loss of Lats2 in mouse embryos caused severe mitotic defects and lethality, indicating that silencing of Lats2 may hinder rather than facilitate cell division (9). Taken together, these data show that silencing of p21Cip1 seems to be the key mechanism underlying such miR-291/294/295–induced tumorigenicity. Nevertheless, our recent efforts to screen the miR-302 target site in human *p21Cip1* gene were futile. Analysis using online microRNA (miRNA) target prediction programs, TARGETSCAN (10) and PICTAR-VERT (11), also showed the same negative outcomes. Therefore, miR-302 and its analogue, miR-291/294/295, likely have different

Authors' Affiliations: [1]WJWU & LYNN Institute for Stem Cell Research, Santa Fe Springs, California and [2]Department of Cell and Neurobiology, Keck School of Medicine, University of Southern California, Los Angeles, California

Note: Supplementary data for this article are available at Cancer Research Online (http://cancerres.aacrjournals.org/).

Corresponding Author: Shi-Lung Lin, WJWU & LYNN Institute for Stem Cell Research, 12145 Mora Drive, STE6, Santa Fe Springs, CA 90670. Phone: 626-236-2885; Fax: 626-294-9950; E-mail: shilungl@mirps.org.

doi: 10.1158/0008-5472.CAN-10-2746

functions in hESCs and mESCs, leading to different characteristics in human and mouse iPSCs. This finding suggests that the model of mouse miR-291/294/295 is inadequate for evaluating miR-302 function in hESCs and human iPSCs.

MiRNA silences its target genes through mismatched binding. Due to this nonstringent interaction feature, miRNA concentration determines the efficiency of gene silencing. To address this dose-dependent miR-302 effect on human iPSC cell cycle, we designed an inducible *pTet-On-tTS-miR302s* expression vector (Fig. 1A, left) to reprogram both normal and cancerous human cells into a pluripotent stem state and then measured the changes in cell proliferation and tumorigenicity. Unlike previous reports using only a single miR-302 member, we placed all four miR-302 familial members, miR-302a, miR-302b, miR-302c, and miR-302d, into one intact cluster (mir-302s; Fig. 1A, right) for simultaneous expression (12). MiRNA microarray analysis revealed that all miR-302 members were efficiently expressed in transfected cells after doxycycline (Dox)-induced stimulation (Fig. 1B). After vector transfection, the biogenesis of miR-302 followed the natural intronic miRNA pathway, in which miR-302s was transcribed with a reporter gene encoding for red fluorescent protein (*RGFP*) and then further spliced into individual miR-302 members by spliceosomal components

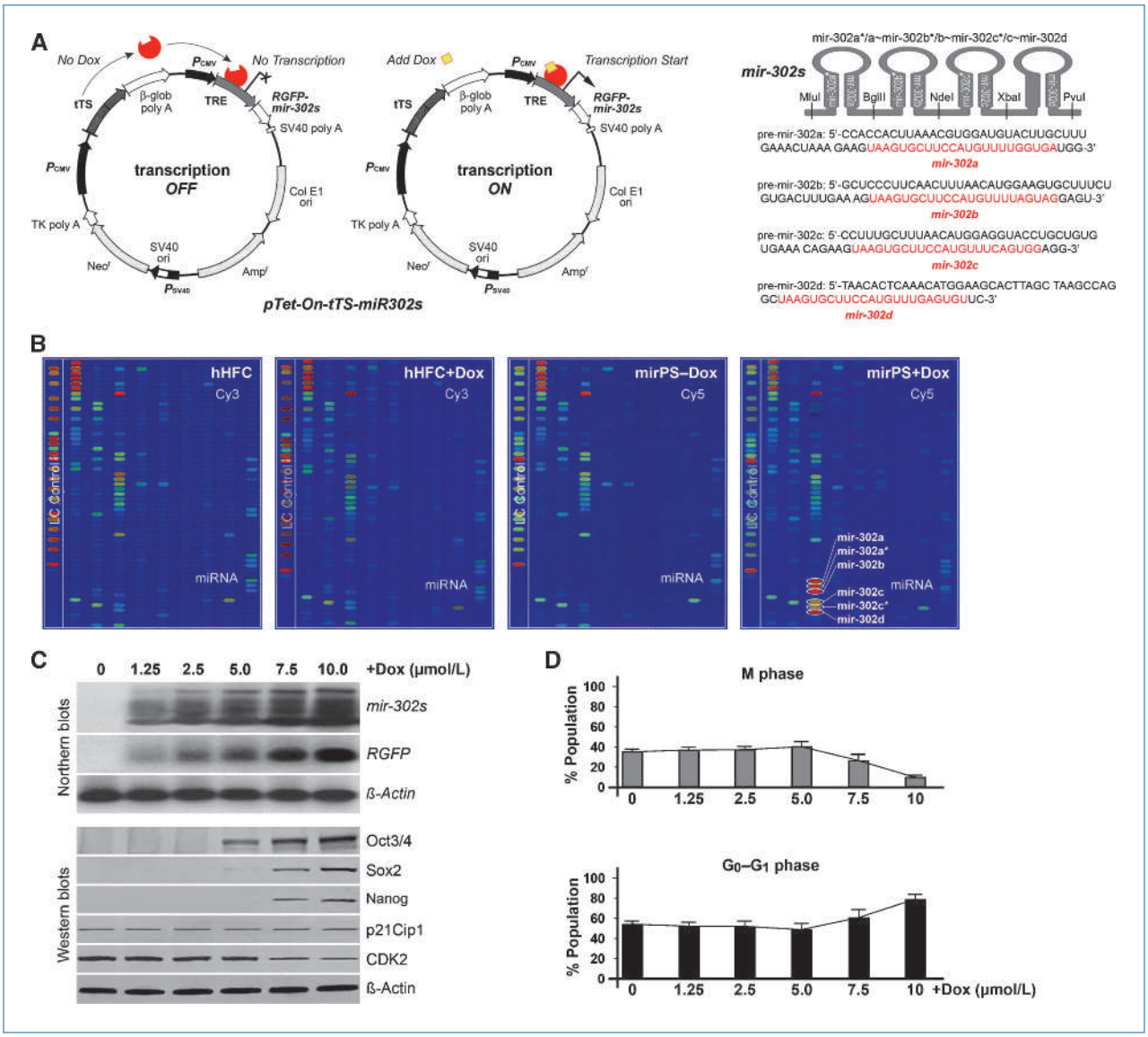

Figure 1. Inducible miR-302 expression and its effect on hHFC proliferation. A, structures of the Dox-inducible *pTet-On-tTS-miR302s* vector (left) and the miR-302 familial cluster (*mir-302s*; right). B, miRNA microarray analysis of induced miR-302 expression at 6 hours after 10 μmol/L Dox treatment ($n = 3$, $P < 0.01$). C, Northern and Western blot analyses of the dose-dependent effect of miR-302 on the expression patterns of the core reprogramming factors Oct3/4-Sox2-Nanog and the hESC-specific cell cycle regulator CDK2 ($n = 5$, $P < 0.01$). D, bar charts of flow cytometry analyses showing the dose-dependent miR-302 effect on the changes of mitotic (M phase) and quiescent (G_0/G_1 phase) mirPS-hHFC populations.

and cytoplasmic RNaseIII Dicers (Supplementary Fig. S1A; ref. 1). The procedure for generating mirPSCs is summarized in Supplementary Fig. S1B. By simulating the natural miR-302 cluster expression pattern in hESCs, our study has unveiled the functional role of this miRNA family in suppressing human pluripotent stem cell cycle and tumorigenicity.

Materials and Methods

Cell culture and electroporation

Cultivation of human normal hair follicle cells (hHFC) and the cancer/tumor cell lines MCF7, HepG2, and Tera-2 was reported in Supplementary Data. hHFCs were isolated from a minimum of two hair dermal papillae. For electroporation, a mixture of *pTet-On-tTS-miR302s* (10 μg) and *pTet-On-Adv-Neo*(−) (50 μg) was added with 20,000 to 50,000 cells in a hypo-osmolar buffer (200 μL; Eppendorf), and electroporation was performed using Eppendorf Multiporator at 300 to 400 V for 150 μs. Treated cells were grown in phenol red–free DMEM (Invitrogen) supplemented with 20% knockout serum, 1% MEM nonessential amino acids, 10 ng/mL bFGF, 1 mmol/L GlutaMax, and 1 mmol/L sodium pyruvate for 24 hours at 37°C under 5% CO_2. Thereafter, 850 μg/mL G418 and >3.75 μg/mL Dox were added and refreshed daily for 3 to 5 days until the cells expressed red fluorescent RGFP. These fluorescent cells (mirPSC) were then selected by fluorescence-activated cell sorting flow cytometry with a monoclonal antibody against the miR-302 expression marker RGFP (Clontech). In the absence of Dox, the selected mirPSCs were grown and passaged in knockout DMEM/F-12 medium (Invitrogen) supplemented with 20% knockout serum, 1% MEM nonessential amino acids, 100 μmol/L β-mercaptoethanol, 1 mmol/L GlutaMax, 1 mmol/L sodium pyruvate, 10 ng/mL basic fibroblast growth factor (bFGF), 100 IU/mL penicillin/100 μg/mL streptomycin/250 μg/mL G418, 0.1 μmol/L A83-01, and 0.1 μmol/L valproic acid (Stemgent) at 37°C under 5% CO_2. Alternatively, in the presence of Dox (3.75–5 μg/mL; Sigma-Aldrich), the mirPSCs were cultivated and passaged in the same feeder-free cultural condition with the addition of 0.05 μmol/L SB216763, a glycogen synthase kinase inhibitor (Stemgent). Treatment with glycogen synthase kinase inhibitor facilitated mirPSC proliferation but with a slight tendency to induce neural differentiation.

Vector construction and routine assays

Methods for constructing the miR-302 familial cluster (*mir-302s*) and inducible *pTet-On-tTS-miR302s* as well as non-inducible *pCMV-miR302s* vectors are reported in Supplementary Data. Routine laboratory preparations and the procedures for Northern blotting, Western blotting, immunostaining, apoptotic DNA laddering, cell invasion, and cell adhesion assays are also described in Supplementary Data.

DNA density flow cytometry

Cells were dissociated by collagenase/trypsin, pelleted, and fixed by resuspension in 1 mL of prechilled 70% methanol in PBS for 1 hour at −20°C. The cells were pelleted and washed once with 1 mL of PBS. The cells were pelleted again and resuspended in 1 mL of 1 mg/mL propidium iodide, 0.5 μg/mL RNase in PBS for 30 min at 37°C. Approximately 15,000 cells were then analyzed on a BD FACSCalibur. Cell doublets were excluded by plotting pulse width versus pulse area and gating on the single cells. The collected data were analyzed using the software package Flowjo using the "Watson Pragmatic" algorithm.

Luciferase 3′-untranslated region reporter assay

Luciferase assays were performed using a modified pMir-Report miRNA Expression Reporter Vector System (Ambion) according to the manufacturer's instruction. Either one or two miR-302 target sites (normal and/or mutant) were inserted in the 3′-untranslated region (UTR) cloning site of the pMir-Report Luciferase Reporter vector. The two target sites were synthesized and separated by 12 -CAGT- repeats. pMir-Report β-gal Control vector was used as a no-reporter control. We transfected 200 ng of the reporter vector into 50,000 mirPSCs in the absence or presence of Dox treatment, using a FuGene HD reagent (Roche Biochemicals), following the manufacturer's suggestion. Cell lysates were harvested 48 hours after transfection, and the knockdown levels of luciferase were normalized and shown by the ratio of relative luciferase activity, which was calculated by the level of luciferase activity in Dox-treated (Dox-on) mirPSCs divided by that of untreated (Dox-off) mirPSCs. Negative control miR-434–expressing cells were generated by electroporating hHFCs with *pTet-On-tTS-miR434-5p* vector.

In vivo tumorigenicity assay

In vivo tumorigenicity assay was performed as reported (13). We xenografted Tera-2 cells (2×10^6 cells in a total volume of 100 μL of Matrigel-PBS) into the flanks (e.g., right hind limb) of 8-week-old male mice (BALB/c nu/nu strain). Tumors were monitored weekly and *in situ* injection of *pCMV-miR302s* or *pCMV-miR302d** vector was conducted 1 week after the Tera-2 xenograft. Five treatments (3-day intervals for each treatment) of 2 μg of polyethylenimine (PEI)-formulated *pCMV-miR302s* or *pCMV-miR302d** vector (total 10 μg) per gram of mouse weight were performed. *In vivo* jetPEI Delivery Reagent (Polyplus-transfection, Inc.) was used following the manufacturer's suggestion. Samples were collected either 3 weeks postinjection or when untreated tumors grew to an average size of approximately 100 mm^3. Major organs, such as blood, brain, heart lung, liver, kidney, and spleen, and the xenografts were removed for histologic evaluation of tumor lesions and immunoreactive cytotoxicity. Tumor formation was monitored by palpation, and tumor volume was calculated using the formula (length × $width^2$)/2. Tumor lesions were counted, dissected, weighed, and subjected to histologic examination using H&E and immunostaining assays. Histologic examination showed no detectable tissue lesions in the brain, heart, lung, liver, kidney, and spleen.

Statistical analysis

Any change over 75% of signal intensity in the analyses of immunostaining, Western blotting, and Northern blotting

was considered as a positive result, which in turn was analyzed and presented as mean ± SE. Statistical analysis of data was performed by one-way ANOVA. When main effects were significant, the Dunnett's post hoc test was used to identify the groups that differed significantly from the controls. For pairwise comparison between two treatment groups, two-tailed Student's *t* test was applied. For experiments involving more than two treatment groups, ANOVA was performed, followed by a post hoc multiple range test. $P < 0.05$ was considered significant. All *P* values were determined from two-tailed tests.

Results

miR-302 attenuates the normal cell cycle rate without causing apoptosis

Our previous studies have shown that increasing miR-302 expression in human melanoma Colo-829 and prostate cancer PC3 cells reprogrammed these malignant cancer cells into a hESC-like pluripotent state (1, 2). During this somatic cell reprogramming (SCR) process, miR-302 induced apoptosis in >98% of the cancer cell population and greatly reduced the proliferation rate of the remaining (<2%) reprogrammed cells. This feature may benefit cancer therapy, yet its effect on normal cells is uncertain. To evaluate this effect, we introduced the inducible *pTet-On-tTS-miR302s* expression vector into normal human hair follicle cells (hHFC). hHFCs were chosen due to their abundance, accessibility, and fast growth. Following an increase of Dox concentration up to 10 μmol/L, we observed that the core reprogramming factors Oct4-Sox2-Nanog were concurrently stimulated at a threshold of Dox ≥7.5 μmol/L, whereas the expression of CDK2 was correspondingly reduced (Fig. 1C). No change of p21Cip1 expression indicated that human p21Cip1 is not a miR-302 target. The mitotic M-phase cell population was reduced by 70% from 37 ± 2% to 11 ± 2%, whereas the quiescent G_0/G_1-phase cell population was increased by 41% from 56 ± 3% to 79 ± 5% (Fig. 1D), reflecting a strong antiproliferative effect similar to our previous observation in miR-302–reprogrammed cancer cells (1). However, most (>95%) of the miR-302–reprogrammed hHFCs (mirPS-hHFC) survived and displayed very limited apoptotic DNA laddering or programmed cell death (Fig. 2A and B), suggesting that normal cells are highly tolerable to the antiproliferative effect of miR-302. It is conceivable that tumor/cancer cells may not survive in such a quiescent state due to their high metabolism and rapid consumption rates.

In the presence of ≥7.5 μmol/L Dox, mirPS-hHFCs presented a quiescent cell morphology (Fig. 2C, red RGFP-positive round cells). Northern blot analysis indicated that the cellular miR-302 concentration in these mirPS-hHFCs was more than 1.3-fold of the level in the hESCs H1 and H9 (Supplementary Fig. S2A). At this specific miR-302 concentration, mirPS-hHFCs strongly expressed Oct3/4, Sox2, Nanog, Lin28, and other major hESC markers (Supplementary Fig. S2A). Microarray analysis of global gene expression further revealed that the transcriptome was changed from a somatic hHFC profile to a hESC-like expression pattern, sharing a total of >93% similarity to H1/H9 cells (Supplementary Fig. S3A). Genomic DNA demethylation, the first sign of SCR, was also detected in these mirPS-hHFCs, resembling the global demethylation patterns observed in H1/H9 cells (Supplementary Fig. S3B and C). Moreover, each individual mirPS-hHFC was able to grow into a single embryoid body with a slow cell cycle rate of approximately 20 to 24 hours (Fig. 2D). We particularly noted that these mirPS-hHFCs were pluripotent but not tumorigenic, as they formed teratoma-like tissue cysts only in the uteri and peritoneal cavities of pseudopregnant female immunocompromised severe combined immunodeficient (SCID)-beige mice. The teratoma-like cysts contained various tissues derived from all three embryonic germ layers: ectoderm, mesoderm, and definitive endoderm (Supplementary Fig. S3D). Alternatively, when xenografted into normal male mice, mirPS-hHFCs were assimilated by the surrounding tissues and expressed the same tissue markers, showing a possible application for regenerating damaged tissues (Supplementary Fig. S2B). Therefore, these findings suggest that miR-302 reprogrammed somatic hHFCs to hESC-like pluripotent stem cells with a relatively slow cell cycle, but not apoptosis.

miR-302 inhibits tumorigenicity and induces apoptosis in various tumor/cancer cells

The findings of miR-302–mediated cancer cell apoptosis and cell cycle attenuation lead us to investigate the possibility of using miR-302 as a universal tumor/cancer drug. Because our previous studies have shown the feasibility of this approach in skin melanoma and prostate cancer cells (1, 2), we further extended our tests to human breast cancer MCF7, hepatocellular carcinoma HepG2, and embryonal teratocarcinoma Tera-2 cells in this study. After *pTet-On-tTS-miR302s* transfection and Dox stimulation, we found that miR-302 induced massive apoptosis in the transfected tumor/cancer cells (Fig. 2A and B). Ectopic miR-302 expression and miR-302–induced Oct3/4-Sox2-Nanog coactivation were confirmed by Northern and Western blot assays, respectively (Supplementary Fig. S4). Flow cytometry analysis comparing DNA content to cell cycle stages further revealed that the apoptotic cell population was increased from 2.6% to 50.1% in mirPS-MCF7, from 1.5% to 39.4% in mirPS-HepG2, and from 2.3% to 29.4% in mirPS-Tera2 cells. The accumulative effect of apoptosis during the whole reprogramming period could eliminate more than 98% of the tumor/cancer cell population. Despite this majority of apoptotic cells, miR-302 reprogrammed a small number (<2%) of the tumor/cancer cells to relatively quiescent mirPSCs that formed embryoid body-like colonies. Compared with their cancer/tumor counterparts, the mitotic cell population in these viable mirPSCs was decreased by 78% from 49 ± 3% to 11 ± 2% in mirPS-MCF7, by 63% from 46 ± 4% to 17 ± 2% in mirPS-HepG2, and by 62% from 50 ± 6% to 19 ± 4% in mirPS-Tera2 cells, whereas the G_0/G_1-phase cell population was increased by 80% from 41 ± 4% to 74 ± 5% in mirPS-MCF7, by 65% from 43 ± 3% to 71 ± 4% in mirPS-HepG2, and by 72% from 40 ± 7% to 69 ± 8% in mirPS-Tera2 cells, respectively (Fig. 3A and B). These results indicate that

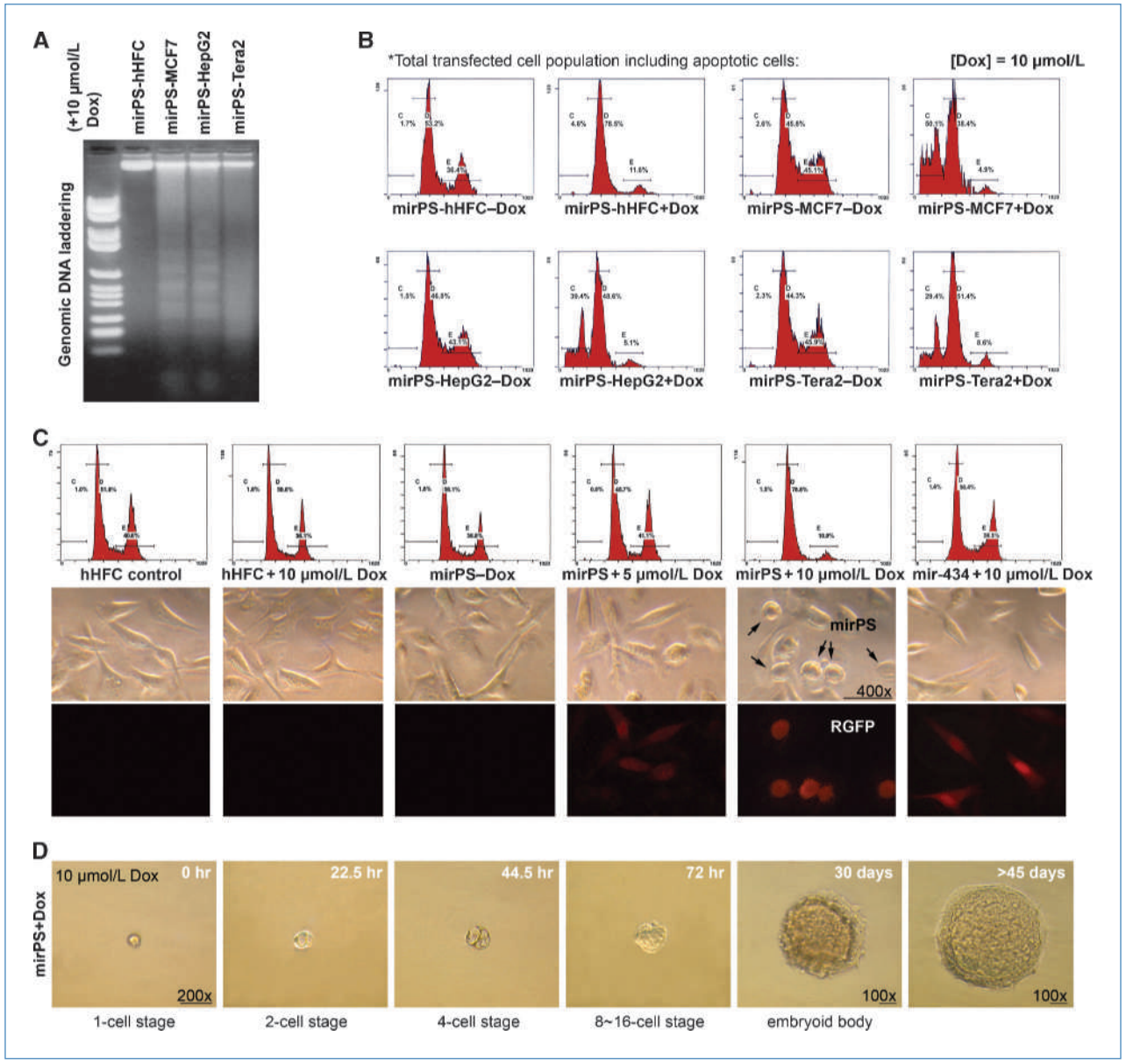

Figure 2. Changes in mirPS-hHFC cell properties following Dox-induced miR-302 expression (Dox, 5 or 10 μmol/L). A, miR-302–induced apoptotic DNA laddering observed in various tumor/cancer-derived mirPSCs, but not in normal hair follicle–derived mirPS-hHFCs. B, comparison of cell apoptosis/proliferation rates between mirPS-hHFCs and other tumor/cancer-derived mirPSCs before and after 10 μmol/L Dox stimulation. Plot charts of flow cytometry analysis show each cell DNA content respective to cell cycle stages, labeled as C (apoptotic cell population), D (G_0/G_1 phase), and E (M phase). C, changes of cell morphology and cell cycle rate before and after miR-302–induced reprogramming in hHFCs ($n = 3$, $P < 0.01$). Bar, 100 μm. D, time course formation of embryoid body from a single mirPS-hHFC after limiting dilution. The cell cycle was estimated to be approximately 20 to 24 h at start but gradually accelerated after 72 h. Bar, 100 μm.

miR-302 effectively inhibited cell proliferation and induced apoptosis in these tumor/cancer cells.

In vitro tumorigenicity assays, using Matrigel chambers (cell invasion assay) and cell adhesion to the human bone marrow endothelial cell (hBMEC) monolayer (cell adhesion assay), revealed two more antitumorigenic effects of miR-302 in addition to its antiproliferative tendencies. Cell invasion assay showed that all three mirPS-tumor/cancer cells lost their ability to migrate (reduced to ~0%), whereas the original tumor/cancer cells aggressively invaded into the chambered areas supplemented with higher nutrients, representing more than 9 ± 3% of MCF7, 16 ± 4% of HepG2, and 3 ± 2% of Tera-2 cell populations (Fig. 3C). Consistently, cell adhesion assay showed that none of these mirPS-tumor/cancer cells could adhere to hBMECs, whereas a significant population of original MCF7 (7 ± 3%) and HepG2 (20 ± 2%)

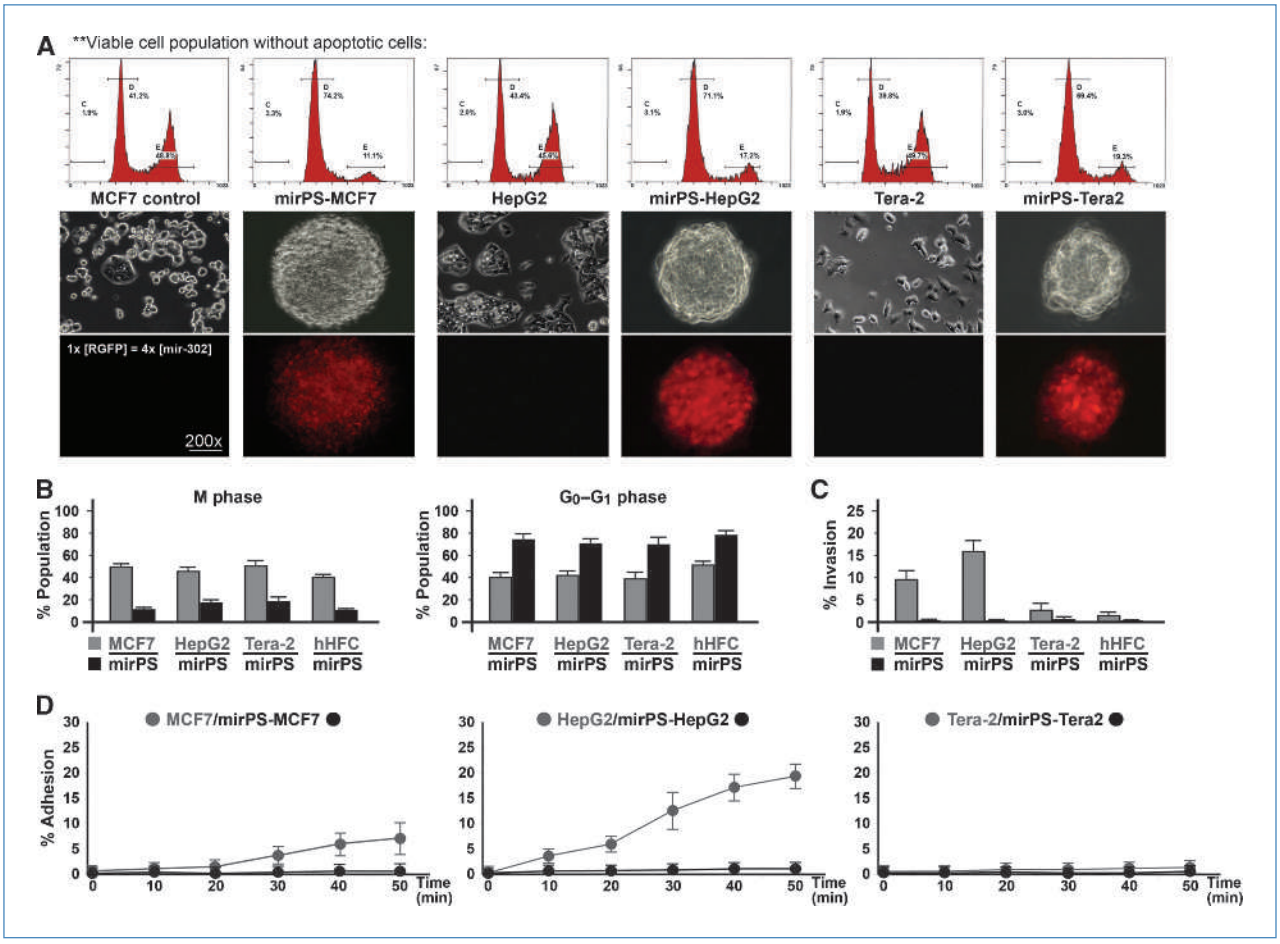

Figure 3. *In vitro* tumorigenicity assays of various tumor/cancer-derived mirPSCs in response to the miR-302 expression induced by 10 μmol/L Dox. A, changes of cell morphology and cell cycle rate between original tumor/cancer cells and their miR-302–reprogrammed mirPSCs, respectively ($n = 3$). Apoptotic cells were excluded to show the mitotic cell population in all viable cells. B, bar charts of flow cytometry analyses showing the dose-dependent miR-302 effects on the changes of mitotic (M phase; $P < 0.01$) and quiescent (G_0/G_1 phase; $P < 0.05$) cell populations of various tumor/cancer-derived mirPSCs. C, functional analysis of miR-302–suppressed tumor invasion in Matrigel chambers ($n = 4$, $P < 0.05$). D, comparison of cell adhesion to the hBMEC monolayer before and after Dox-induced miR-302 expression ($n = 4$, $P < 0.05$).

cells quickly metastasized onto the hBMEC monolayer after a 50-min incubation period (Fig. 3D). Taken together, all of the findings thus far strongly and repeatedly show that miR-302 is a human tumor suppressor capable of attenuating fast cell growth, causing tumor/cancer cell apoptosis, inhibiting tumor/cancer cell invasion, and preventing metastasis. Most importantly, this novel miR-302 function may offer a universal treatment against a multitude of human cancers and tumors, such as malignant skin, prostate, breast, and liver cancers and various forms of tumors.

miR-302–mediated antiproliferation functions through cosuppression of CDK2, cyclin D1/D2, and BMI-1

To validate the direct interactions between miR-302 and its target sites in G_1-phase checkpoint regulators, we used a luciferase 3′-UTR reporter assay (Fig. 4A) to measure the inhibitory effects of different miR-302 concentrations on the target sites of *CDK2, cyclin D1/D2*, and *BMI1 polycomb ring finger oncogene* (*BMI-1*). In the presence of 10 μmol/L Dox, miR-302 effectively bound to these target sites and successfully silenced >80% of the reporter luciferase expression in all targets (Fig. 4B). Consistent with this result, suppression of the real target genes in mirPSCs was also confirmed by Western blot analysis (Fig. 4C). In contrast, a lower miR-302 concentration induced by 5 μmol/L Dox failed to trigger any significant silencing effect (>50%) on either the target sites of the reporter gene or the targeted G_1-phase checkpoint regulators (Fig. 4B and D), indicating that miR-302 modulates the cell cycle rate in a dose-dependent manner. Given that the G_1-S phase transition of mammalian cell cycle is normally controlled by two compensatory cyclin-CDK complexes, cyclin D-CDK4/6 and cyclin E-CDK2 (14), we found that miR-302 over a certain threshold concentration is able to inactivate both complexes through simultaneous suppression of CDK2 and cyclin D1/D2 activities, thereby blocking both G_1-S transition pathways and attenuating the

cell cycle rate of the reprogrammed mirPSCs. In hHFCs and mirPSCs, cyclin D3 was expressed at an insufficient level to compensate for the loss of cyclin D1/D2 in the mirPSCs.

Accompanying miR-302–mediated BMI-1 silencing, we further detected a mild increase in p16Ink4a and p14Arf expression (gain of 63 ± 17% and 57 ± 13% of the levels in hHFCs, respectively), whereas no change was observed in p21Cip1 expression (Fig. 4C). Deficiency of BMI-1, an oncogenic cancer stem cell marker, has been shown to inhibit G_1-S cell cycle transition through enhancement of p16Ink4a and p14Arf tumor suppressor activities (15). In this scenario, 16Ink4a directly inhibits cyclin D–dependent CDK4/6 activity through phosphorylation of retinoblastoma protein Rb and thus prevents Rb from inducing the E2F-dependent transcription required for S-phase entry (16, 17). In addition, p14Arf prevents HDM2 from binding to p53 and permits the p53-dependent transcription responsible for G_1 arrest or apoptosis (18). However, because knockdown of CDK2 has been shown to be sufficient to arrest hESCs at G_1 phase (19), silencing of BMI-1 as well as coactivation of p16Ink4a and p14Arf in mirPSCs may offer an extra function in suppressing SCR-associated tumorigenicity, of which the mechanism remains to be determined.

Treatment of miR-302 eliminates >90% of teratoma cell growth *in vivo* without changing stem cell pluripotency

After understanding the tumor suppressor mechanism of miR-302, we tested the use of miR-302 as a drug for treating

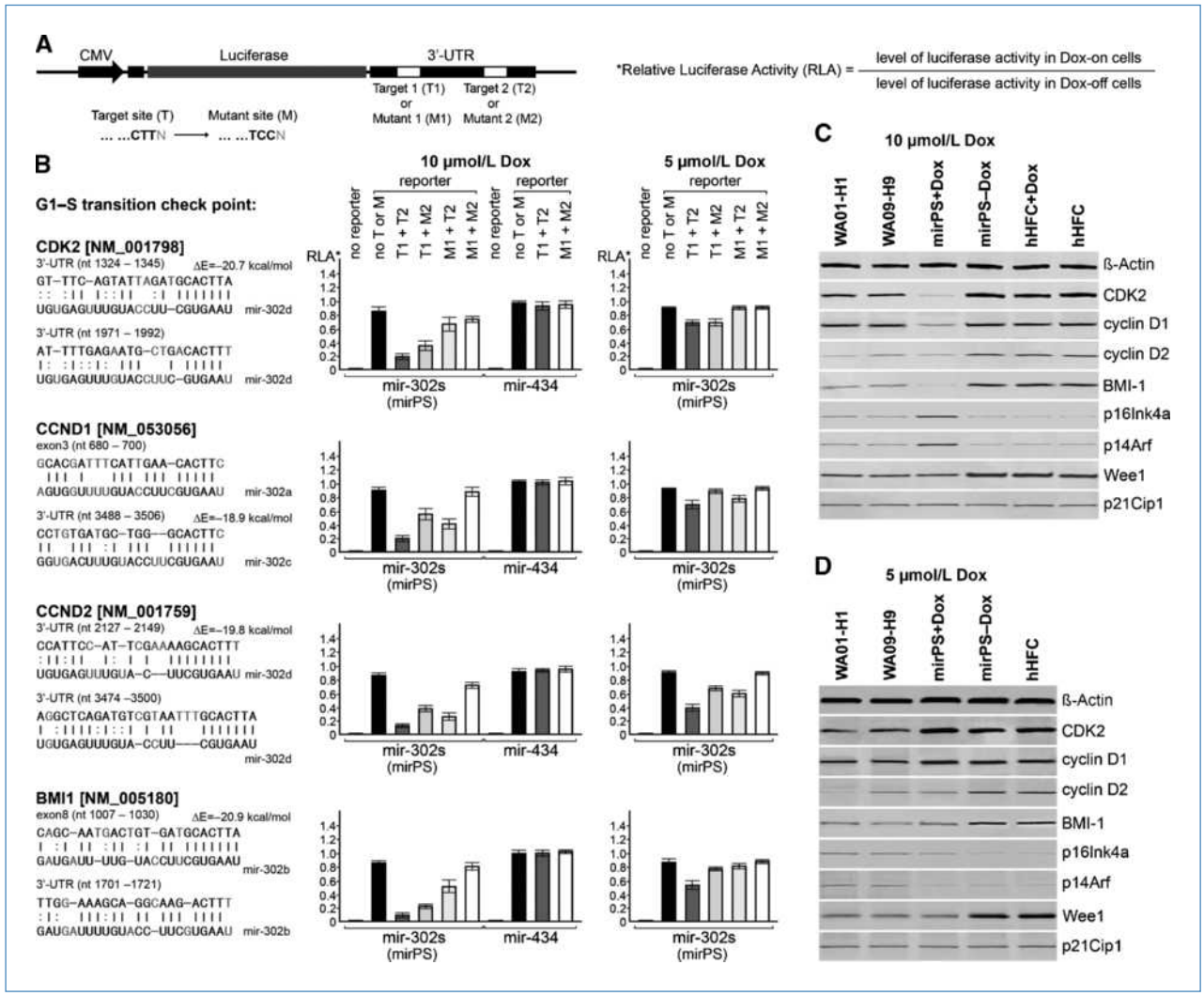

Figure 4. Luciferase 3′-UTR reporter assays of miR-302–induced gene silencing effects on targeted G_1-phase checkpoint regulators. A, constructs of the luciferase 3′-UTR reporter genes, which carried either two normal (T1 + T2) or two mutant (M1 + M2), or a mixture of both (T1 + M2 or M1 + T2), miR-302 target sites in the 3′-UTR. The mutant sites contained a mismatched TCC motif in place of the uniform 3′-CTT end of the normal target sites. B, effects of Dox-induced miR-302 elevation on the luciferase expression ($n = 5$, $P < 0.01$). Dox = 5 or 10 μmol/L. CCND1 and CCND2 refer to cyclin D1 and cyclin D2, respectively. C and D, Western blot analyses showing the changes of major miR-302–targeted G_1-phase checkpoint regulators induced by high (10 μmol/L Dox) and low (5 μmol/L Dox) miR-302 concentrations in mirPSCs compared with those found in the hESCs H1 and H9 ($n = 4$, $P < 0.01$).

Tera-2–derived teratomas in 8-week-old male athymic mice (BALB/c nu/nu strain). Tera-2 cells are pluripotent human embryonal carcinoma (hEC) cells that can differentiate into a variety of somatic tissues *in vivo*, in particular primitive glandular and neural tissues (20). Due to its pluripotency, Tera-2–derived teratoma may serve as a model for treating various tumor types *in vivo*. For drug delivery, we adopted *in situ* injection of PEI-formulated *pCMV-miR302s* expression vector in close proximity to the tumor site. The *pCMV-miR302s* vector was formed by changing the *TRE*-controlled *CMV* promoter to a regular *CMV* promoter, of which the expression duration was approximately 1 month in human cells due to DNA methylation. By injecting up to 10 μg of the *pCMV-miR302s* vector per gram of mouse weight (the maximal amount for single injection in a mouse), we observed no signs of sickness or cachexia in all tested mice, indicating the safety of this approach.

We detected a significant inhibitory effect on teratoma growth after five treatments (3-day intervals for each treatment) of 2 μg of *pCMV-miR302s* vector (total 10 μg) per gram of mouse weight. As shown in Fig. 5A, treatment with the *pCMV-miR302s* vector resulted in a marked decrease of the average teratoma size by >89% (11 ± 5 mm^3; $n = 6$) compared with that of nontreated ones (104 ± 23 mm^3; $n = 4$). In contrast, treatment with the same amount of PEI-formulated antisense-miR-302d expression vector (*pCMV-miR302d**) increased the average teratoma size by 140% (250 ± 73 mm^3; $n = 3$). Tera-2 cells were known to express a moderate amount of miR-302 (Fig. 5B). Northern blotting confirmed that miR-302 expression levels were inversely correlated with the teratoma sizes (Fig. 5B), suggesting that modulating cellular miR-302 expression is an effective means to control the growth of teratomas *in vivo*. We also performed Western blotting to show the cosuppression of CDK2-cyclin D1/D2-BMI-1 and the coactivation of the core reprogramming

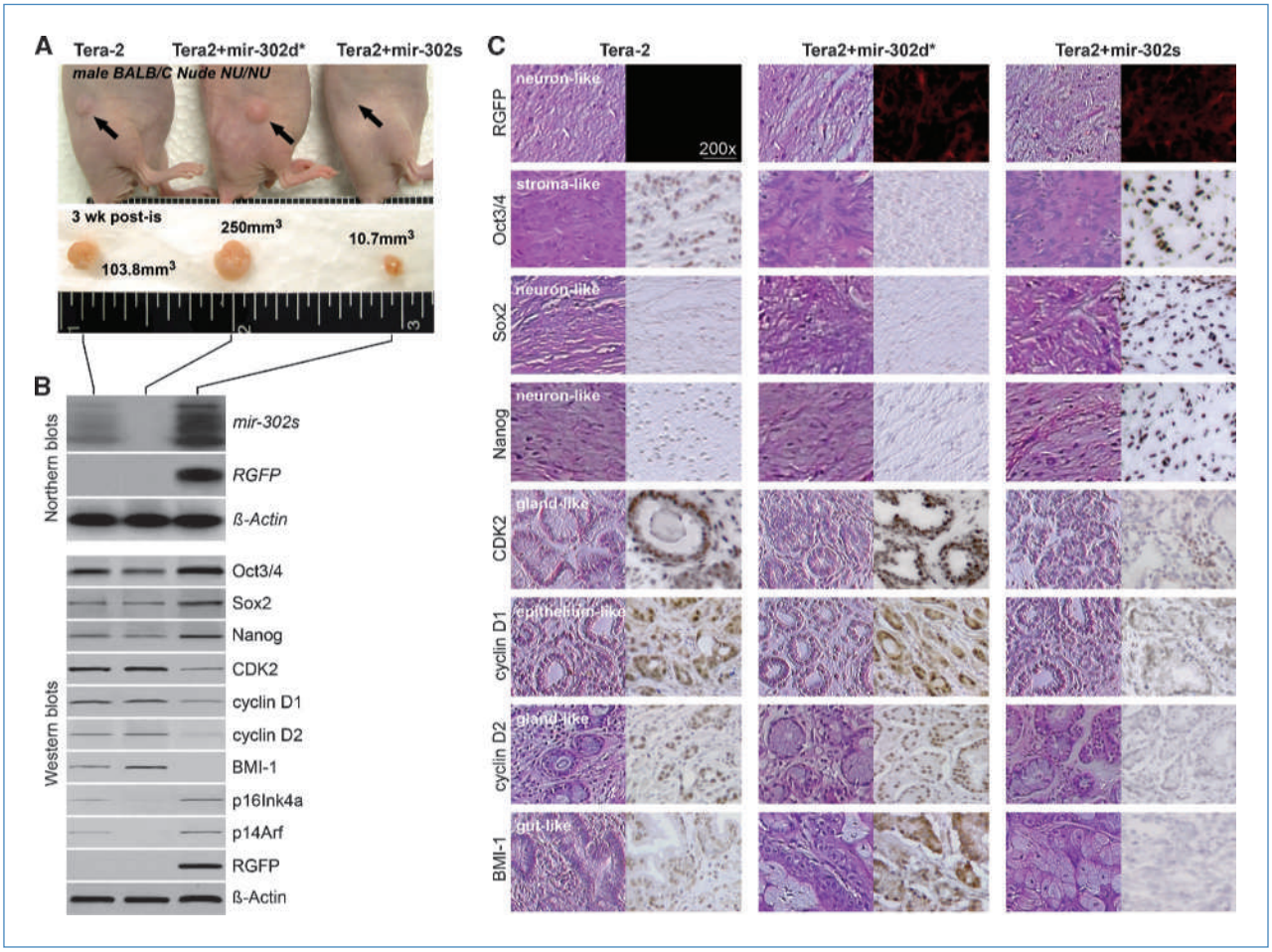

Figure 5. *In vivo* tumorigenicity assays of mirPS-Tera2 cells in response to constitutive miR-302s (Tera2 + mir-302s) or miR-302d* (Tera2 + mir-302d*) expression ($n = 3$, $P < 0.05$). miR-302s and miR-302d* were transcribed from the *pCMV-miR302s* and *pCMV-miR302d** vectors in the transfected Tera-2 cells, respectively. A, morphologic evaluation of average tumor sizes 3 wk after *in situ* injections (post-is). All tumors were localized in the original implant sites (black arrows). No signs of cachexia or tumor metastasis were observed in all tested mice. B and C, Northern and Western blot analyses (B) and immunohistochemical staining analyses (C) of the *in vivo* miR-302 effect on the expression patterns of the core reprogramming factors Oct3/4-Sox2-Nanog and the miR-302–targeted G_1-phase checkpoint regulators CDK2, cyclin D1/D2, and BMI-1 as well as p16Ink4a and p14Arf.

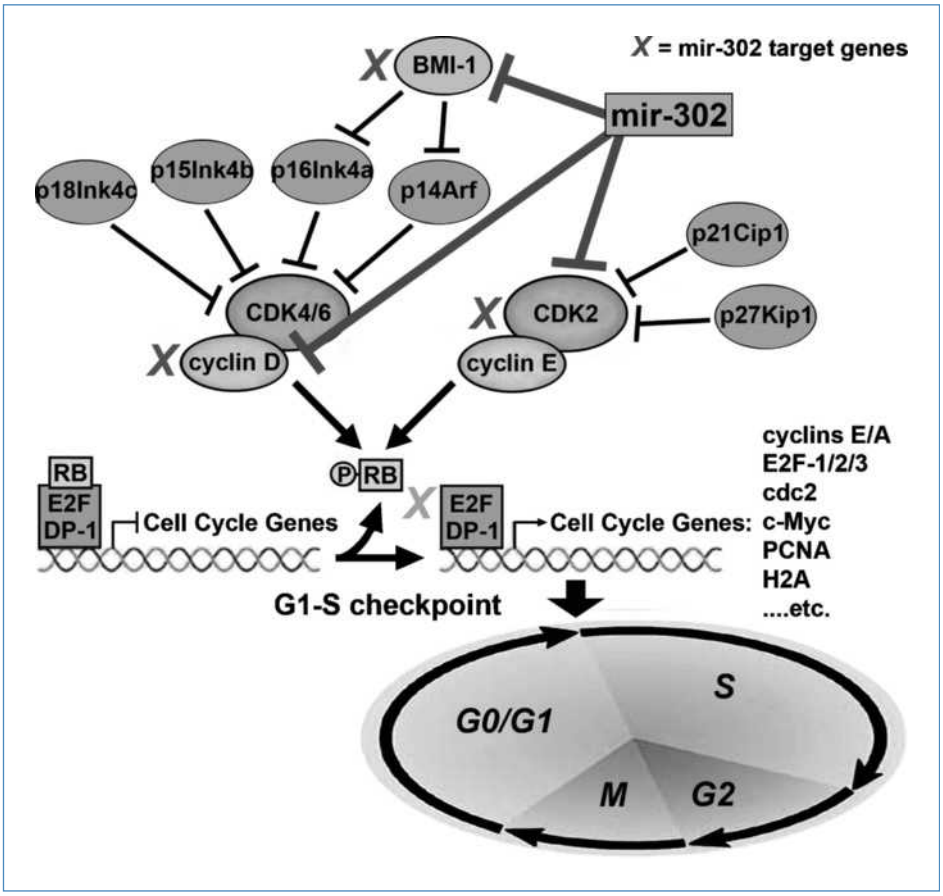

Figure 6. Proposed mechanism of miR-302–mediated cell cycle regulation in human cells. miR-302 not only concurrently suppresses the G_1-phase checkpoint regulators CDK2, cyclin D1/D2, and BMI-1 but also activates p16Ink4a and p14/p19Arf to quench most (>80%) of the cell cycle activities during SCR. E2F is also a predicted target of miR-302. Relative quiescence at the G_0/G_1 state may prevent possible random growth and/or tumor-like transformation of the reprogrammed pluripotent stem cells, leading to a more accurate and safer reprogramming process, by which premature cell differentiation and tumorigenicity are both inhibited.

factors Oct3/4-Sox2-Nanog in the *pCMV-miR302s*-treated teratomas (Fig. 5B), consistent with the previous findings *in vitro* (Figs. 1C and 4C). The same results were further confirmed by immunohistochemical staining for respective proteins in teratoma tissue sections (Fig. 5C). Most noteworthily, we found that miR-302 inhibited teratoma cell growth without affecting its nature in pluripotent differentiation, indicating that miR-302 plays a dual role in tumor suppression and SCR. Based on this dual function of miR-302 and our validation *in vitro* and *in vivo*, we conclude that the same antiproliferative mechanism of miR-302 observed *in vitro* can be applied to inhibit teratoma growth *in vivo*, which may serve as a potential treatment for a variety of human tumors. This finding also explains why mirPSC implantation preferably forms teratoma-like tissue cysts in the uteri of pseudopregnant SCID-beige mice (ref. 1; Supplementary Fig. S3D), which may secrete certain growth/differentiation factors to reduce the antiproliferative effect of miR-302.

Discussion

The stringency of miRNA-mRNA interaction determines the real function of a miRNA. Different cellular conditions may affect the way of miRNA-mRNA interaction to change the preference of miRNA-mediated gene targeting. However, there is currently no report related to either the dose-dependent effect of miR-302 or the stringency of miR-302-target interaction. Our study provides important insights on these issues and, for the first time, revealed that miR-302 functions differently between humans and mice. In humans, miR-302 strongly targets *CDK2, cyclin D1/D2*, and *BMI-1*, but not *p21Cip1*. Unlike mouse *p21Cip1*, human *p21Cip1* does not contain any target site for miR-302. This difference in gene targeting leads to a significant schism between respective cell cycle regulations. In mESCs, miR-302 silences mouse p21Cip1 to promote cell proliferation (7, 21), whereas in humans, p21Cip1 expression is preserved and may reduce cell proliferation. In addition, we found that miR-302 suppresses BMI-1 to slightly stimulate p16Ink4a/p14ARF expression. Because p16Ink4a and p14ARF are elevated while p21Cip1 remains unchanged in human mirPSCs, the antiproliferative and antitumorigenic effects of miR-302 likely result from a synergistic mechanism involving the suppression of cyclin E-CDK2 and cyclin D-CDK4/6 activities and the activation of p16Ink4a-Rb and p14/19Arf-p53 cell cycle regulations. This distinct miR-302–mediated mechanism in human pluripotent stem cells is fundamentally different from the previously reported p21Cip1 silencing in mESCs. Therefore, the previous mouse model cannot explain the miR-302 function in human cells.

miR-302–induced SCR and cell cycle attenuation are two collateral events dependent on the cellular miR-302 concentration. We observed that both events occur almost simultaneously at a miR-302 concentration more than 1.3-fold the level found in hESCs H1/H9, indicating that this specific concentration is the minimal threshold for initiating both events. Previous studies using a single miR-302 member at a miR-302 concentration below this threshold failed to effectively elicit SCR and cell cycle attenuation. Furthermore, we have shown in this study that the miR-302 concentration induced by 5 μmol/L Dox failed to silence the target sites of the reporter gene as well as the targeted G_1-phase checkpoint regulators. Comparatively, early embryonic cells before the morula stage (32–64 cell stage) often exhibit a relatively slow cell cycle rate, similar to that of mirPSCs, whereas such stringent cell cycle regulation is not found in late blastocyst–derived hESCs. We therefore hypothesized that a lower miR-302 concentration in blastocyst-derived hESCs may not be sufficient to silence the targeted G_1-phase checkpoint regulators and oncogenes. This also explains why hESCs have dramatic proliferative ability and tend to form tumors instead. However, the real reason may never be unveiled due to the restriction and controversy on stem cell research using early embryonic cells.

In sum, our studies show that miR-302–mediated cell cycle regulation involves a highly coordinated mechanism between cosuppression of multiple G_1-phase checkpoint regulators and activation of CDK inhibitors. All genetic events of this mechanism must occur simultaneously to prevent any rapid G_1-S progression. Relative quiescence at G_0/G_1 phase cell cycle is an important step for reprogrammed pluripotent stem cells to adapt their new hESC-like state and subsequently prevent tumorigenic transformation. Through deciphering the interactions between miR-302 and its target genes, we propose here the intricate mechanism for miR-302–associated cell cycle regulation during SCR, as shown in Fig. 6. We have previously shown that miR-302 silences its targeted epigenetic regulators to activate Oct3/4-Sox2-Nanog coexpression and induce SCR (1). In this study, we further showed that miR-302 concurrently silences CDK2, cyclin D1/D2, and BMI-1 to attenuate cell division during SCR. The inhibition of BMI-1 also enhances the tumor suppressor activities of p16Ink4a and p14/p19Arf in the reprogrammed cells. Proper control of the cell cycle rate is of critical biological importance in preventing the tumorigenicity of oncogenes that are often activated during SCR. Through these synergistic cell cycle regulation pathways, miR-302 is able to initiate SCR while preventing stem cell tumorigenicity.

Disclosure of Potential Conflicts of Interest

No potential conflicts of interest were disclosed.

Received 07/27/2010; revised 08/30/2010; accepted 09/16/2010; published OnlineFirst 11/09/2010.

References

1. Lin SL, Chang D, Chang-Lin S, et al. Mir-302 reprograms human skin cancer cells into a pluripotent ES-cell-like state. RNA 2008; 14:2115–24.
2. Lin SL, Ying SY. Role of mir-302 microRNA family in stem cell pluripotency and renewal. In: Ying SY, editor. Current perspectives in microRNAs. New York: Springer Publishers; 2008, p. 167–85.
3. Takahashi K, Yamanaka S. Induction of pluripotent stem cells from mouse embryonic and adult fibroblast cultures by defined factors. Cell 2006;126:663–76.
4. Yu J, Vodyanik MA, Smuga-Otto K, et al. Induced pluripotent stem cell lines derived from human somatic cells. Science 2007;318: 1917–20.
5. Wernig M, Meissner A, Foreman R, et al. *In vitro* reprogramming of fibroblasts into a pluripotent ES-cell-like state. Nature 2007;448: 318–24.
6. Card DA, Hebbar PB, Li L, et al. Oct4/Sox2-regulated miR-302 targets cyclin D1 in human embryonic stem cells. Mol Cell Biol 2008;28: 6426–38.
7. Wang Y, Baskerville S, Shenoy A, Babiarz JE, Baehner L, Blelloch R. Embryonic stem cell-specific microRNAs regulate the G_1-S transition and promote rapid proliferation. Nat Genet 2008;40:1478–83.
8. Deng C, Zhang P, Harper J, Elledge S, Leder P. Mice lacking p21Cip1/Waf undergo normal development, but are defective in G_1 checkpoint control. Cell 1995;82:675–84.
9. Yabuta N, Okada N, Ito A, et al. Lats2 is an essential mitotic regulator required for the coordination of cell division. J Biol Chem 2007;282: 19259–71.
10. TargetScanHuman release 5.1 [homepage on the Internet]. Cambridge (MA): Whitehead Institute for Biomedical Research; c2006–2009 [updated 2009 April;cited 2010 July 27]. Available from: http://www.targetscan.org/.
11. PICTAR-VERT [homepage on the Internet]. New York: Center for Comparative Functional Genomics; c2005–2007 [updated 2007 March 26; cited 2010 July 27]. Avaliable from: http://pictar.mdc-berlin.de/cgi-bin/PicTar_vertebrate.cgi/.
12. Suh MR, Lee Y, Kim JY, et al. Human embryonic stem cells express a unique set of microRNAs. Dev Biol 2004;270:488–98.
13. Lin SL, Chang D, Ying SY. Hyaluronan stimulates transformation of androgen-independent prostate cancer. Carcinogenesis 2007;28: 310–20.
14. Berthet C, Klarmann KD, Hilton MB, et al. Combined loss of Cdk2 and Cdk4 results in embryonic lethality and Rb hypophosphorylation. Dev Cell 2006;10:563–73.
15. Jacobs JJ, Kieboom K, Marino S, DePinho RA, van Lohuizen M. The oncogene and Polycomb-group gene bmi-1 regulates cell proliferation and senescence through the ink4a locus. Nature 1999; 397:164–8.
16. Parry D, Bates S, Mann DJ, Peters G. Lack of cyclin D-Cdk complexes in Rb-negative cells correlated with high levels of p16INK4/MTS1 tumor suppressor gene product. EMBO J 1995;14:503–11.
17. Quelle DE, Zindy F, Ashmun RA, Sherr CJ. Alternative reading frames of the NK4a tumor suppressor gene encode two unrelated proteins capable of inducing cell cycle arrest. Cell 1995;83:993–1000.
18. Kamijo T, Zindy F, Roussel MF, et al. Tumor suppression at the mouse INK4a locus mediated by the alternative reading frame product p19ARF. Cell 1997;91:649–59.
19. Neganova I, Zhang X, Atkinson S, Lako M. Expression and functional analysis of G_1 to S regulatory components reveals an important role for CDK2 in cell cycle regulation in human embryonic stem cell. Oncogene 2009;28:20–30.
20. Andrews PW, Damjanov I, Simon D, et al. Pluripotent embryonal carcinoma clones derived from the human teratocarcinoma cell line Tera-2. Differentiation *in vivo* and *in vitro*. Lab Invest 1984;50:147–62.
21. Judson RL, Babiarz JE, Venere M, Blelloch R. Embryonic stem cell-specific microRNAs promote induced pluripotency. Nat Biotechnol 2009;27:459–61.